IMPEDANCE CHARACTERIZATION AND MODELING OF MICROELECTRODES FOR NEURAL RECORDING

Marcelo Bariatto Andrade Fontes
Catholic University of Leuven, Division of Neurophysiology,
Herestraat 49 – bus 1021, 3000 Leuven, Belgium.
Bariatto.Fontes@med.kuleuven.be
On leave from
Faculdade de Tecnologia de São Paulo
FATEC-SP/CEETEPS - São Paulo, Brasil.

Abstract

Electrode-electrolyte impedance is one of important characteristic for neural recording applications due to its influence on the signal/noise ratio and signal distortion. In this work a model of the electrode-electrolyte is described and validated through electrochemical impedance spectroscopy technique (EIS), using commercial platinum and platinum/iridium alloy microelectrodes used in acute neural recording. The impedance of the electrodes was measured in standard physiological saline solution (0.9% NaCl). A two electrode setup was used in which the working electrode was connected to the microelectrodes and the counter electrode was short-connected to the reference (stainless steel). The data was collected using an electrochemical analyzer (CompactStat, IviumTechnologies).In order to address the behavior of the electrode impedance an equivalent circuit of the electrode/electrolyte interface has been modeled. Since the impedance is strongly dependent on the electrode area, electrochemical characterization of the area was also performed using a standard iron ferricyanide solution – $K_3Fe(CN)_6$.

Keywords: microelectrodes, impedance spectroscopy, electrochemical characterization

Introduction

In the neural recording, the bioelectric potentials carried in electrolytic media in form of ionic currents, are transduced by the electrodes in to electronic signals. This takes place by means of capacitive coupling (without net charge transfer) and by charges transfer reaction in which the electrodes and ions in the physiologic environment exchange electrons through redox reactions [1].

Electrochemical impedance spectroscopy (EIS) has been used to characterize the behavior of the electrode/electrolyte interface, contributing to developing its electrical model and therefore improving the electrode design to achieve the desired interface properties for biomedical applications [2,4].

The area of the electrode plays a major role in the signal/noise ratio leading to a trade-off [5] since the detected neuron signal decreases as the electrode area increases due to the ionic current spreading and also reduces the thermal noise due to impedance decreasing.

In this paper it is presented the impedance modeling and validated by using commercial platinum and platinum/iridium alloy microelectrodes used in acute neural recording.

Equivalent circuit model

Considering the potential amplitude involved in neuron activity recording – microvolts - a small signal equivalent model of the electrode can be considered at equilibrium (or quasi-equilibrium), where mainly the capacitive properties of the electrode are considered and it behaves like a network of linear circuit elements [1-4].

The I x V curve or I x η (the out of equilibrium potential or overpotential) for an redox reaction is describe through the Butler-Volmer equation (1) as showed in figure 1, that can be simplified for small signals (η < 0.01 V) leading to the Ohmic form equation (2). This corresponds to the first term of the electrical model, the transfer resistance Rt, which is the slope^{-1} in curve. Equation 2 can be rewritten in terms of current density (J) and electrode area (A), so Rt scales with A^{-1}, equation 3.

$$i_{total} = i_a - i_c = i_o \left(e^{\frac{\frac{1}{2}\eta q}{kT}} - e^{-\frac{\frac{1}{2}\eta q}{kT}} \right) \quad (1)$$

$$\eta < 0.01V \Rightarrow i_{total} \approx i_o \frac{q}{kT}\eta \quad (2)$$

$$R_t = \frac{\eta}{i_{total}} = \frac{\frac{kt}{q}}{i_0} = \frac{V_T}{J_o A} \quad (3)$$

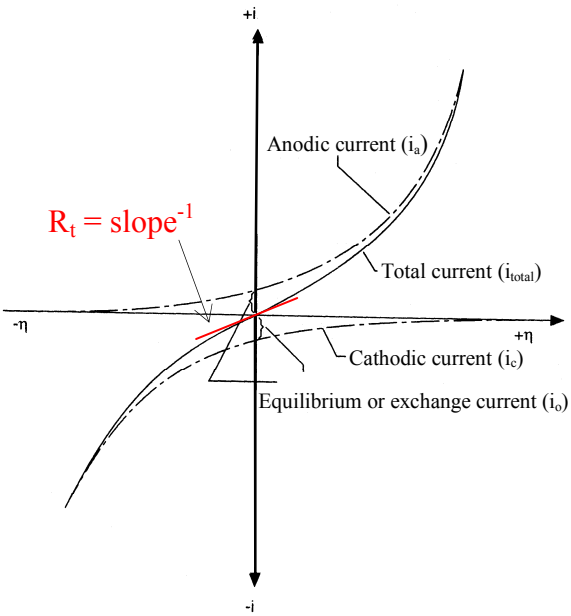

Figure 1. Current vs. overpotential for a redox reaction described by Butler-Volmer equation which can be simplified as an Ohmic equation for η < 0.01 V (red straight line).

The electrified electrode creates an interfacial ionic distribution (figure 2) modeled by Guy-Chapman–Stern theory resulting in the Helmholtz capacitance (C_H, equation 4), that is purely a parallel capacitor with dielectric constant ε_r (water), in series with the Guy-Chapman capacitance (C_G, equation 5) that takes into account the diffused ionic distribution, which depends on the applied voltage (V), the number of electrons exchanged in the redox reaction (z) and the ionic concentration (N_i). The association of these two capacitances leads to the interface capacitance C_I, which is, clearly, proportional to the electrode area, therefore its impedance goes with $(A.f)^{-1}$, where f is the signal frequency, equation 6.

The interfacial capacitance is the major factor in the small signal model.

$$C_H = \frac{\varepsilon_0 \varepsilon_r A}{d_{OHP}} \tag{4}$$

$$C_G = \frac{\varepsilon_0 \varepsilon_r A}{L_D} \cosh\left(\frac{zV}{2V_T}\right) \qquad L_D = \sqrt{\frac{\varepsilon_0 \varepsilon_r V_T}{2N_i z^2 q}} \tag{5}$$

$$\frac{1}{C_I} = \frac{1}{C_H} + \frac{1}{C_G} \qquad \left|z_{C_I}\right| = \frac{1}{2\pi f C_I} \tag{6}$$

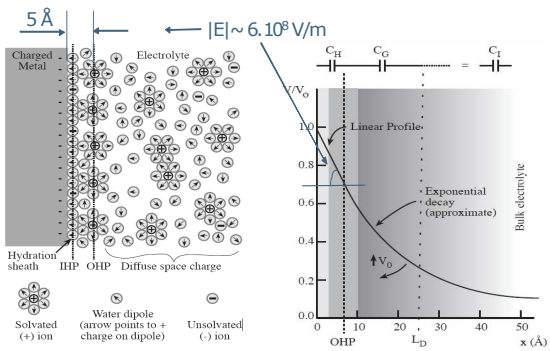

Figure 2. Ionic distribution close to an electrified electrode modeled as two capacitors.

Up to now the ionic diffusion were not taken in account and since it is a time demanding process (square root), it will be frequency dependent. This would bring an extra change in the resistance and capacitance (Warburg impedance) – equation 7, that indeed varies by the square root of frequency. More accurate analysis shows f^{α} ($0.22<\alpha<0.79$) [6]. The Warburg impedance impacts more as low the frequency goes, as the equation suggests, also one can observed that R_w scales with A^{-1} and $|Z_{CW}|$ goes with $(f.A)^{-1}$.

$$R_W = \frac{V_T}{2z^2 AqNi\sqrt{\pi f D}} \qquad C_W = \frac{z^2 AqNi}{V_T}\sqrt{\frac{D}{\pi f}} \tag{7}$$

What were discussed applied for all electrodes immersed in an electrolyte. Therefore the same evaluation should be done for the auxiliary electrode or counter electrode (the second electrode for the EIS), but since it is chosen with a very large area its impedance can be neglected at first approximation. In the other hand, the distance between the detection electrode and auxiliary electrode can not be neglected, since the electrolyte resistance (R_s) has to be in to account. Equation 8 describes R_s for circular electrode which scales with $A^{-1/2}$.

$$R_S = \frac{\rho\sqrt{\pi}}{4\sqrt{A}} \tag{8}$$

Other aspect is the electrode self potential or half-cell potential, which is a constant value not considered for the EIS (ac analysis).

The electrical circuit model, called Randles model, is presented in the figure 3. For very low frequencies the electrode impedance magnitude is expected to follow (R_t+R_W+R_s). In the other hand at high frequencies only R_s should be measured and for intermediary frequencies the impedance of the capacitor C_i would represent the major electrode component, therefore decreasing its impedance with the frequency. Furthermore, the electrode impedance magnitude should decrease with the electrode area. The impedance phase should be zero for the frequencies where the resistances are the major component and close to ninety degrees in the capacitance range.

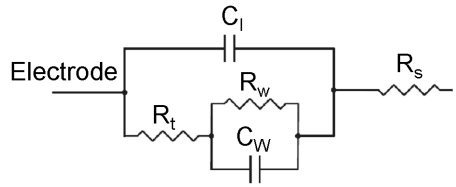

Figure 3. Electrical circuit model for the electrode/electrolyte interface (Randles circuit).

Table 1. Values adopted for the electrode/electrolyte interface electrical model.

Property	Value
□□□F/m□□□	8.853E-12
□r (water) =	7.943E+01
d OHP (m) =	5.000E-10
z =	1
VT (V) =	2.542E-02
Vp (V) =	5.00E-02
q (C) =	1.602E-19
Temp (oC) =	22
Temp (F) =	295.15
[NACl] % v/v =	0.9
[NACl] Molar =	1.538E-01
k (J/K) =	1.380E-23
N0 =	6.022E+23
Ni (ions /m3)=	9.265E+25
J0 (A/m2) =	8.50E-04
Difussion coef (m2/s) =	4.00E-09
Resistivity (Ohm*m) =	7.20E-01

Figure 4 shows an example of simulated magnitude and phase impedance for a platinum electrode (Φ=50µm). The expected behavior discussed previously is observed. The influence of each component in the total magnitude impedance is presented in figure 5. For frequencies between 10mH and 10KHz the interfacial capacitance represents the impedance magnitude, and outside of this range the resistances are more important. It can also be observed that the Warburg component has a minor influence in the total value and can be neglected at first approximation. For the simulation, MS Excel and LT Spice were used based on the values listed in Table 1.

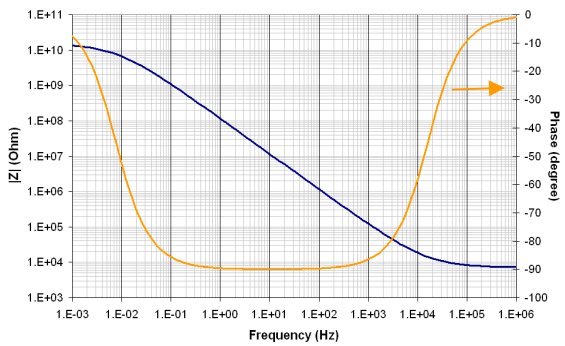

Figure 4. Simulated impedance magnitude and phase for Φ=50µm platinum electrode.

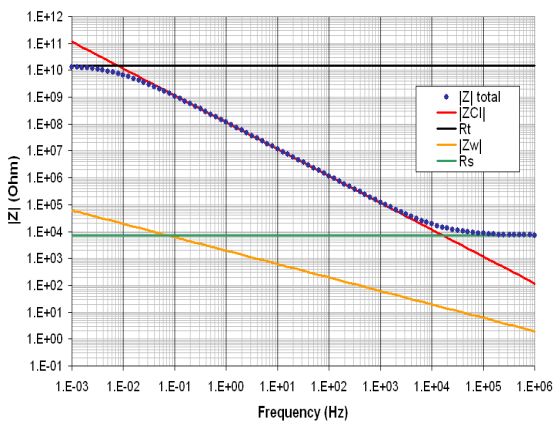

Figure 5. Parameters of the Randles model in the electrode impedance magnitude.

The impedance magnitude at four different electrode diameters is presented in the figure 6. The increasing in the electrode area reduces its impedance. This can better seen in the figure 7, where electrode impedance magnitude seems to scale as $|Z| \propto A^{-1}$, at any frequency.

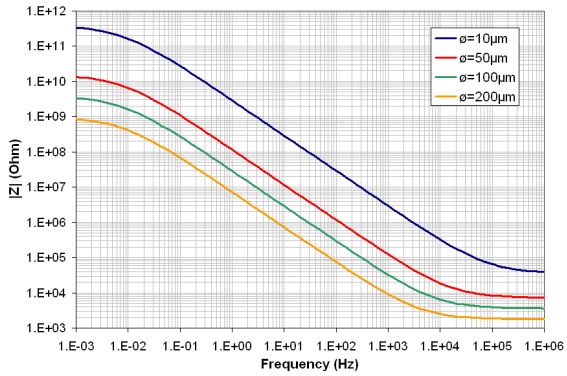

Figure 6. Impedance magnitude for several electrode diameters.

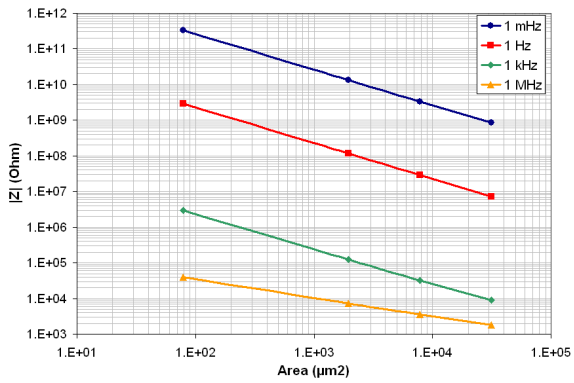

Figure 7. Impedance magnitude variation with electrode area.

Since the electrode area has a strong impact on its impedance the next section will discuss the determination of the electrode area through electrochemical experiments which take into account its active area.

Electrode area determination

Electrochemical determination of the electrode area was carried out either using Cyclic Voltammetry (CV) or ChronoAmperometry (CA) techniques.

For CV, the relationship between the current peak, for a reduction or oxidation reaction, and the electrode area (A) is given by the Randles-Sevcik [7,8], equation 9, where n represents the number of electron involved in the redox reaction, D is the diffusion coefficient of the ions in solution, C is its concentration and ν represents the scan rate.

$$I_p = 2.69.10^5 .n^{3/2}.A.D^{1/2}.C.v^{1/2} \qquad (9)$$

In the other hand for CA, it was used the procedure developed by Denuault et al. [9,10] for

the determination of the diffusion coefficient of an electroactive species. If the number of electrons involved in the electrochemical step is known, then the concentration of the solution can be calculated by using the steady state current value. According to these authors, for relatively long time experiments (0.05 > t > 10 s), a plot of the dependence of the normalized current (the ratio between the current measured at time t and the steady state current) versus $t^{-1/2}$, gives a straight line which slope is proportional of the electrode radius r, equation 10.

$$\frac{I_t}{I_{ss}} = 1 + \left(\frac{2}{\pi^{3/2}}\right) . r . \frac{1}{\sqrt{(Dt)}} \qquad (10)$$

Experimental

Electrochemical Impedance Spectroscopy, Cyclic Voltammetry and Chronoamperometric techniques were carried out by an electrochemical analyzer (CompactStat, Ivium Technologies) on commercial platinum electrode (Φ=100µm, BASi®) and platinum-iridium alloy wire electrodes used for neural recording (FHC®). Those former probes can have different tip geometry and are fabricated to achieve a desired impedance at given frequency. All electrodes were cleaned before used by acetone, followed by isopropyl alcohol and finally rinsed in DI water. Alumina polishing (1µm) could be used only for platinum electrode. Stainless steel "large" electrode was used as auxiliary electrode.

All experiments were performed in standard physiological saline solution (0.9% NaCl – Braun®), as shown in figure 8. For CV and CA, 10 mM/L of potassium ferricyanide solution in 0.1 M/L NaCl were used.

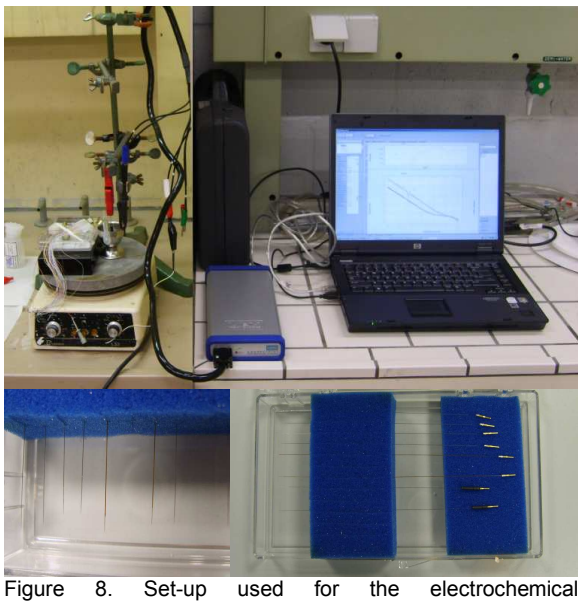

Figure 8. Set-up used for the electrochemical characterizations. It is also shown some microelectrodes for neural recording.

Results

The CV voltammogram after the 5th cycle is presented in the figure 9, for the platinum electrode, before and after polishing with alumina. It can be seen clearly the influence of the cleaning process in the electrode response for the redox reaction. Calculations using equation 8 leads to an increase of around 11% in the electrode diameter: form 89µm to 99µm.

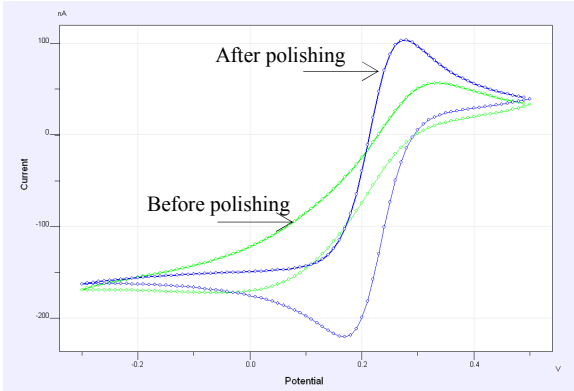

Figure 9. Cyclic voltammograms of potassium ferricyanide at Φ=100µm platinum electrode, before and after polishing, after the 5th cycle.

Similarly results were obtained using chronoamperometry, figure 10, with advantage of using only one voltage step to perform the experiment. In this case the diameter changed from 87µm to 101µm.

Alternatively way to also estimate the electrode area can done by using impedance spectroscopy at high frequencies, where the solution resistance is the major factor. Calculation using equation 8 leads to a diameter of 99µm.

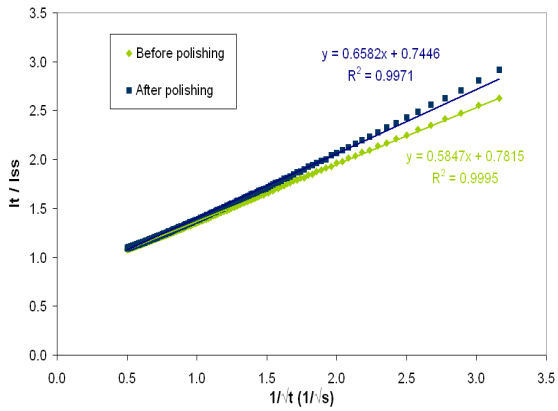

Figure 10. Cronoamperometric results of potassium ferricyanide at Φ=100µm platinum electrode, before and after polishing.

Impedance spectroscopy results are presented in figure 11. It can be seen a reduction on the impedance, for frequencies below 100KHz, due to increase of the electrode active area after the cleaning process. Some 50Hz noise was also detected.

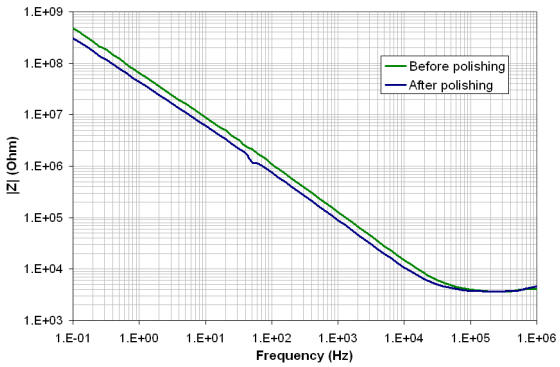

Figure 11. Impedance magnitude recorded before and after the platinum electrode polishing (Φ=100µm).

The same characterization was performed for platinum/iridium alloy microelectrodes used in acute neural recording. Figure 12 presents the voltammogram compared with platinum electrode. Since the current peak is proportional to the electrode area, equation 8, the results clearly indicates that the acute microelectrode has smaller active area, 192µm^2 or a diameter equivalent of 15.6µm.

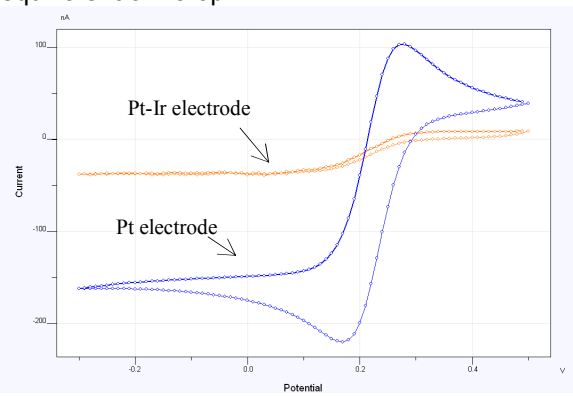

Figure 12. Cyclic voltammograms of potassium ferricyanide at Pt-Ir electrode compared with platinum electrode (Φ=100µm), after the 5th cycle.

From the previous analysis, the impedance magnitude for the platinum/iridium alloy is expected to be higher than for the platinum electrode. Actually the specifications for this type of electrode say that it should presents 1MΩ at 1KHz. Indeed this was obtained experimentally, as shown in figure 13.

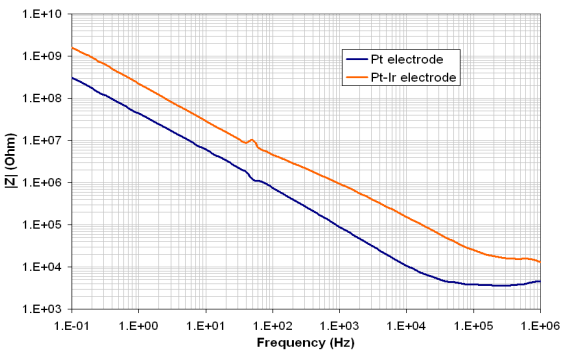

Figure 13. Cyclic voltammograms of potassium ferricyanide at Pt-Ir electrode compared with platinum electrode (Φ=100µm), after the 5th cycle.

The next step is to compare the experimental impedance with simulation using the obtained electrode area. Figure 14 shows the results for the platinum electrode. One can observed that at frequencies lower than 10Hz the model overestimated the experimental data, probably due to the uncertainness in the value used for the exchange current density (j_0) – equation 3 – which is very sensitive to the electrode surface properties. For frequencies higher that 1MHz, cable parasitic capacitance influences the signal, which was not considered into the model.

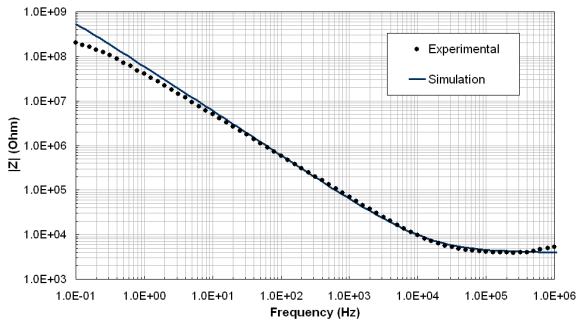

Figure 14. Simulated and experimental; results for the impedance magnitude of the platinum electrode (Φ=100µm).

Similar results could be achieved for the platinum/iridium neural electrode, figure 15. In this case, the simulated data showed more deviation if compared with the previous case. This can be related with the oxidation of the electrode surface, due to the lack of mechanical polishing, not possible for this kind of electrode. This is reinforced due to the clearly capacitive behavior of the electrode for all frequency range.

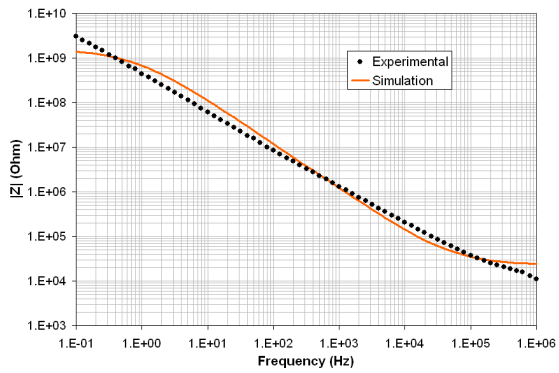

Figure 15. Simulated and experimental; results for the impedance magnitude of the platinum/iridium neural electrode (area=192µm^2).

Conclusion

The simple description of the electrode-electrolyte model presented here (Randles circuit), combined with electrochemical impedance spectroscopy and electrochemical determination of the active electrode area provide a valid tool to help electrode design in biomedical applications.

Acknowledgments

The author wish to acknowledge Siddharth Srivastava from KULeuven for the neural electrodes and the Interuniversity Microelectronics Center (IMEC) for the infrastructure.

References

[1] G.T.A. Kovacs, "Microelectrode models for neural interfaces," in Enabling Technologies for Cultured Neural Networks (D.A. Stenger and T.M. McKenna, Eds.), pp. 121-165, Academic Press, New York, 1994.
[2] W. Franks, I. Schenker, P. Schmutz, and A. Hierlemann, "Impedance characterization and modeling of electrodes for biomedical applications," IEEE Trans. Biomed. Engineering, vol. 52, no. 7, pp. 1295-1302, July 2005.
[3] Macdonald, J.R. editor, "Impedance Spectroscopy: Emphasizing Solid Materials and Systems, John Wiley & Sons, 1987.
[4] David A. Borkholder, Cell Based Biosensors Using Microelectrodes, PhD. Dissertation, Stanford University, 1998.
[5] Lempka, S. F. & all. "Optimization of Microelectrode Design for Cortical Recording Based on Thermal Noise Considerations" EMBS Annual International Conference New York City, USA, Aug 30-Sept 3, 2006.
[6] Geddes, L.A., Electrodes and the measurement of bioelectric events, John Wiley & Sons, Inc., London (1972)
[7] G. A. Mabbott, An Introduction to Cyclic Voltammetry, Journal of Chemicals Education, Set. 1983, Vol. 60, No. 9, pp 697-701.
[8] A.J. Bard, and L.R. Faulkner, Electrochemical Methods, John Wiley & Sons, Inc., New York, 1980.
[9] G. Denuault, M. V. Mirkin and A. J. Bard, J. Electroanal. Chem.,1991, 308, 27.
[10] J.O'M. Bockris and A.K.N. Reddy, Modern Electrochemistry, Plenum Press, New York, 1970.